

Explainable AI-Driven Neural Activity Analysis in Parkinsonian Rats under Electrical Stimulation

Jibum Kim^{a,c,1}, Hanseul Choi^{a,1}, Gaeun Kim^{b,1}, Sunggu Yang^{b,c}, Eunha Baeg^{b,c}, Donggwe Kim^{b,c}, Seongwon Jin^a and Sangwon Byun^{d,*}

^aDepartment of Computer Science and Engineering, Incheon National University, Yeonsu-gu, 22012, Incheon, Republic of Korea

^bDepartment of Nanobioengineering, Incheon National University, Yeonsu-gu, 22012, Incheon, Republic of Korea

^cCenter for Brain-Machine Interface, Incheon National University, Yeonsu-gu, 22012, Incheon, Republic of Korea

^dDepartment of Electronics Engineering, Incheon National University, Incheon National University, Yeonsu-gu, 22012, Incheon, Republic of Korea

¹Jibum Kim, Hanseul Choi and Gaeun Kim are contributed equally to this work.

*Corresponding author:

Sangwon Byun

Department of Electronics Engineering, Incheon National University, Incheon, Korea

Email: swbyun@inu.ac.kr, Phone: +82 32 835 8451, Fax: +82 32 850 5519

Abstract

Parkinson's disease (PD) is a neurodegenerative disorder characterized by motor dysfunction and abnormal neural oscillations. These symptoms can be modulated through electrical stimulation. Traditional neural activity analysis in PD has typically relied on statistical methods, which often introduce bias owing to the need for expert-driven feature extraction. To address this limitation, we explore an explainable artificial intelligence (XAI) approach to analyze neural activity in Parkinsonian rats receiving electrical stimulation. Electrocorticogram (ECoG) signals were collected before and after electrical stimulation using graphene-based electrodes that enable less-invasive monitoring and stimulation in PD. EEGNet, a convolutional neural network, classified these ECoG signals into pre- and post-stimulation states. We applied layer-wise relevance propagation, an XAI technique, to identify key neural inputs contributing to the model's decisions, incorporating the spatial electrode information matched to the cortex map. The XAI analysis highlighted area-specific importance in β and γ frequency bands, which could not be detected through mean comparison analyses relying on feature extraction. These findings demonstrate the potential of XAI in analyzing neural dynamics in neurodegenerative disorders such as PD, suggesting that the integration of graphene-based electrodes with advanced deep learning models offers a promising solution for real-time PD monitoring and therapy.

Keywords: Explainable AI (XAI), Machine Learning, Electrocorticogram (ECoG), Parkinson's Disease Detection, Layer-wise Relevance Propagation, Convolutional Neural Network, Brain-Computer Interface

1. Introduction

Parkinson's disease (PD), affecting approximately 1% of individuals over the age of 60, is a neurodegenerative disorder primarily caused by the degeneration of the dopaminergic system [1]. PD patients experience a range of motor dysfunctions, such as tremors, rigidity, bradykinesia, and postural instability [2]. A popular contemporary clinical treatment for PD is deep brain stimulation (DBS), i.e., electrically stimulating the subthalamic nucleus and globus pallidus interna to alleviate motor symptoms [3,4]. However, although DBS can reduce symptoms such as tremors, it is an invasive method. DBS can damage non-targeted brain regions during electrode implantation; furthermore, removing deeply implanted electrodes poses considerable challenges. In addition, continuous electrical stimulation requires a physician's supervision whenever PD symptoms manifest. With these concerns in mind, less invasive therapeutic approaches and methods for real-time monitoring of PD are needed.

We have developed graphene-based electrodes that are biocompatible, electrically conductive, thermally stable, and mechanically flexible [5]. These properties make graphene electrodes well-suited for recording neural activity related to brain disorders and brain mapping, as they minimize tissue damage and inflammatory responses after implantation [5,6,7,8]. Furthermore, our graphene electrode arrays can be integrated with wireless microprocessors so that they can measure brain activity and deliver electrical stimulation without movement restrictions. This combined wireless system can offer a less traumatic procedure, allowing easier real-time monitoring and treatment of brain disorders.

One of the key features of PD is abnormal oscillatory neural activity, particularly in high-frequency bands, such as β and γ , which show increased activity [9]. Interestingly, electrical stimulation such as DBS has been shown to reverse these patterns by reducing high-frequency oscillations [10,11], suggesting that neural activity can be tracked to evaluate the therapeutic potential of electrical stimulation in modulating abnormal brain activity. Therefore, using less-invasive methods such as graphene electrodes to continuously monitor brainwave changes and provide the corresponding stimulation therapy is expected to contribute to the treatment of the disease substantially.

To fully harness this potential, it is essential to analyze brain activity recorded through these advanced electrodes accurately. Traditionally, the analysis of brain activity, typically through electroencephalogram (EEG) or electrocorticogram (ECoG) signals, has relied on

statistical methods. These approaches have been extensively used in PD research, including studies that reveal abnormal oscillatory activity in high-frequency bands [9]. However, statistical techniques often require expert-driven feature extraction, which can introduce bias in the results [12]. With the recent rise of artificial intelligence, new opportunities have emerged to apply deep learning techniques, including Explainable AI (XAI), to physiological signals like EEG and ECoG, in order to reduce the bias problems inherent in traditional statistical methods [13,14,15]. XAI-based methods can analyze the signals without the need for feature extraction by experts, thereby reducing the potential bias introduced by human factors and other hyperparameters that may influence the results [12]. Despite these advantages, analyses of ECoG signals obtained from the Parkinsonian rat model have typically relied on traditional statistical methods with limited application of XAI techniques. While hardware advancements such as graphene electrodes can play a crucial role in PD treatment research, introducing deep learning and XAI can also offer novel interpretations of the results.

Our study aims to address existing gaps by exploring the feasibility of applying XAI methods to analyze ECoG signals acquired using graphene-based electrodes in a Parkinsonian rat model. Specifically, we employ EEGNet, a lightweight convolutional neural network (CNN) architecture designed for EEG classification tasks [16]. This model has consistently demonstrated high performance across various applications, including motor imagery and sleep stage classification, making it a key advancement in brain-computer interface (BCI) technology [17]. In addition to EEGNet, we apply layer-wise relevance propagation (LRP), a prominent XAI technique, to explain which inputs contribute most significantly to the model's outputs. LRP performs backpropagation through the model layers, propagating relevance scores to the input layer and identifying the specific input values influencing the model's decisions. LRP has been successfully used in previous neuroimaging studies, such as the classification of Alzheimer's disease using MRI data [18].

In this study, we apply LRP to the EEGNet model to compare brain activity before and after electrical stimulation in the Parkinsonian rat model, using graphene-based electrodes for signal acquisition. By comparing these XAI-based findings with results from traditional statistical methods, we aim to highlight the distinct advantages of XAI in producing unbiased insights into PD-related neural activity. Our results suggest that the proposed XAI methods can provide a reliable understanding of brain activity in PD without depending on expert-driven feature extraction, thereby advancing hardware and analytical approaches for the treatment and

study of neurodegenerative disorders.

2.1. Materials and Methods

2.1.1. Animals

Each of four adult male Sprague Dawley rats (260–300 g) was labeled with an identifier: PD1, PD2, PD3, and PD4. The rats were accommodated in a facility whose temperature was set at 25°C and subjected to a 12-hour light/dark cycle. All animal procedures were approved by the Institutional Animal Care and Use Committee at Incheon National University (Approval Code: INU-ANIM-2017-08) in accordance with their guidelines, and all experiments were conducted in compliance with the ARRIVE guidelines.

2.1.2. 6-OHDA-induced hemiparkinsonian rat model

To establish a pharmacologically induced PD model in animals, 6-hydroxydopamine (6-OHDA) was stereotactically injected into the dopaminergic neurons of the medial forebrain bundle. Under isoflurane anesthesia, a single burr hole was made in rats at coordinates -3.84 mm anterior and -1.4 mm lateral relative to the bregma. A solution containing 2.94 mg of 6-OHDA in saline and 0.1% ascorbic acid was injected using a Hamilton syringe (26G needle) with a micro-pump (LMS Korea, Seongnam, Gyeonggi, Republic of Korea) at a depth of 8.5 mm from the dura. The infusion was administered at a rate of 0.5 μ l/min over a period of 8 minutes into one hemisphere, allowing for a straightforward comparison with the non-affected hemisphere, which served as the control. Three weeks following 6-OHDA administration, the rats were injected with apomorphine (0.5 mg/kg), and an apomorphine-induced rotation test was performed for 30 minutes to confirm the induction of PD. Rats that exhibited at least three full-body rotations per minute were considered to have successfully developed the model.

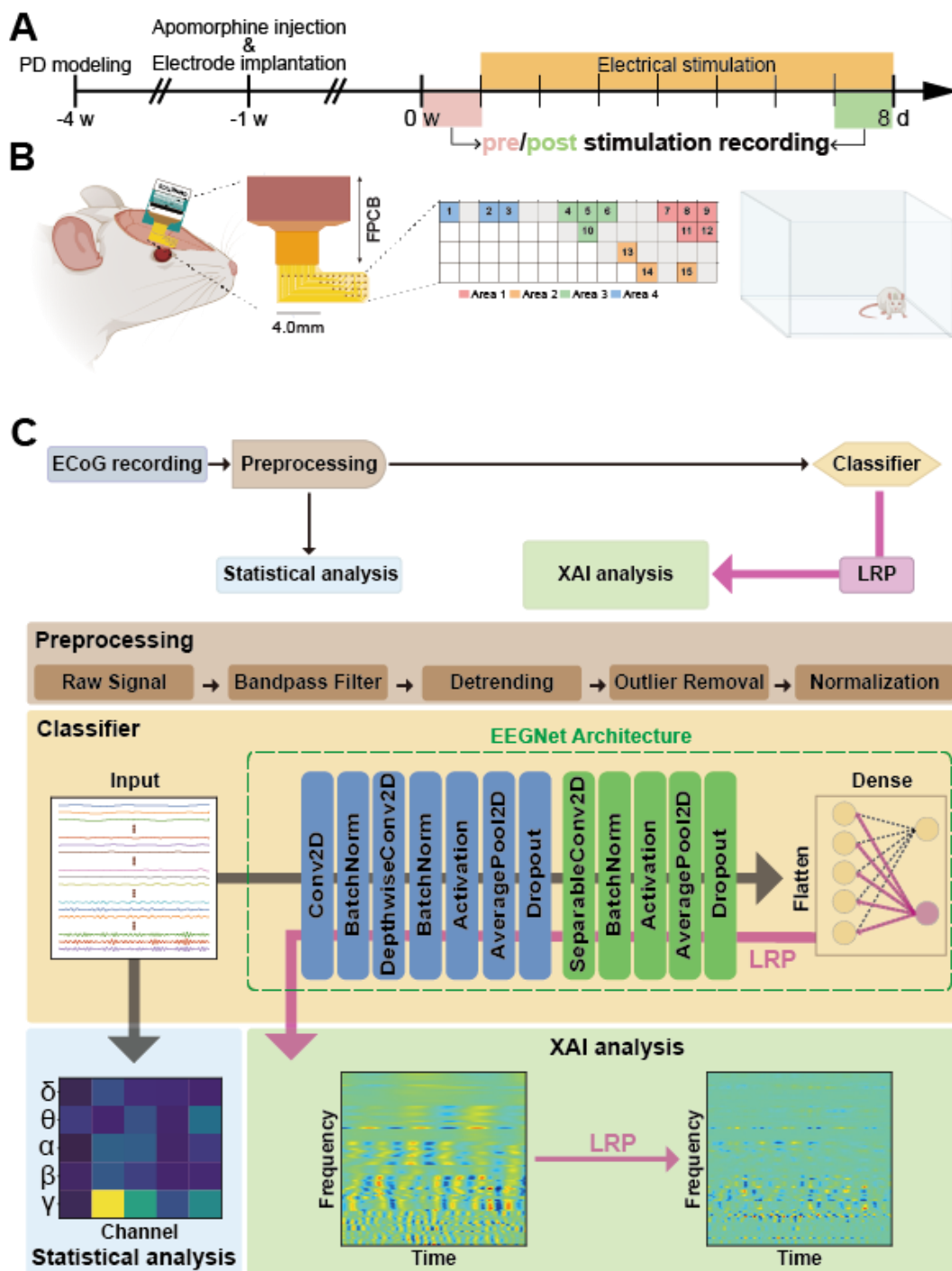


Figure 1. Overall experimental procedure. (A) Timeline for PD modeling and ECoG measurement process. (B) Electrode configuration and placement. The left diagram illustrates the shape and positioning of each electrode (numbered), along with the grouping of the channels based on the motor cortex map. The right illustration shows a rat in its natural, unrestrained state during ECoG recording. (C) Schematic of the overall framework post-signal recording, including signal preprocessing, statistical analysis, classifier application, and XAI analysis.

2.1.3. Graphene-based electrode fabrication

We utilized the same technique employed in our previous studies to create a graphene-based electrode array [4,12,7,8,5]. Monolayer graphene grown on Cu foil through chemical vapor deposition (CVD) was stacked into four layers following the chemical doping process. A 1.2- μm -thick polyimide (PI) layer was deposited by spin-coating onto a copper carrier substrate, forming a flexible printed circuit board (FPCB). For the interconnects, a layer of Cr/Au (3 nm/40 nm) was applied onto the PI layer using thermal evaporation followed by photolithography. The four-layer graphene was then transferred onto the PI substrate, aligned with the Au contact tracks, and shaped using photolithography combined with oxygen plasma treatment. SU-8 was used to insulate the undesired areas of the Au tracking metal. The graphene was subsequently patterned and etched using photolithography and oxygen plasma, followed by nitric acid chemical doping.

2.1.4. Experimental designs for electrotherapy and recording

In animals confirmed to have PD via the apomorphine-induced rotation test, a graphene-based electrode array integrated with an Omnetics connector (Gbrain, Incheon, Korea) was surgically implanted onto the motor cortex of the affected hemisphere. The array was encapsulated by the skull and securely anchored using dental cement. Electrical stimulation was delivered directly to the motor cortex, with stimulation sessions beginning one-week post-implantation. The Parkinsonian rats received an hour of electrical stimulation (biphasic, 130 Hz, 66.6 μs , 300 μA) daily for 8 consecutive days (Figure 1A) in order to evaluate its therapeutic effects over an 8-day period. Stimulation was controlled using an RHS stim/recording controller (INTAN Technologies, Los Angeles, CA, USA), which was connected to the implanted electrode via a head stage and an 8-Mbit/s serial peripheral interface cable (INTAN Technologies, Los Angeles, CA, USA). Figure 1B shows a rat implanted with the head stage and electrodes.

Neural activity was recorded using a wireless device, as described below. ECoG signals from the motor cortex were recorded for 30 minutes prior to the first stimulation as well as after the final stimulation using a 15-channel graphene-based electrode array. The channels were grouped into four areas based on the motor cortex map (Figure 1B): Area 1 (channels 7, 8, 9, 11, and 12) corresponding to the face, Area 2 (channels 13, 14, and 15) corresponding to

the forelimb, Area 3 (channels 4, 5, 6, and 10) corresponding to the trunk, and Area 4 (channels 1, 2, and 3) corresponding to the hindlimb [26]. All recordings were conducted in freely moving, awake Parkinsonian rats within a 43×33×30 cm cage placed inside a Faraday cage, without food, water, or objects present during measurements. (Figure 1B).

2.1.5. Wireless device

The proposed neuroprosthetic device delivers short-latency electrical stimulation driven by physiological signals and operates autonomously via wireless telemetry. Designed specifically for animal models, the device is optimized for minimal size, weight, and power consumption. The system incorporates a lightweight 3.8-g head stage, integrating critical functions such as stimulation, recording, telemetry, power management, and on-device computing through a dedicated microprocessor. It utilizes Bluetooth Low Energy (BLE) 4.0 for wireless data transmission, ensuring high data integrity through sample sequence values that maintain precise timing, even during intermittent connection losses.

2.2. Signal Preprocessing

Given that brain wave data is susceptible to various noise sources, such as environmental noise or the subject's movement, it is necessary to remove noise before analysis. Given that the rats were freely moving during the measurements, the likelihood of movement-induced noise was higher compared to stationary or anesthetized subjects. Therefore, in addition to the commonly used bandpass or notch filters, we incorporated two more preprocessing steps: detrending and outlier removal [19].

The 30-min long wirelessly recorded signals were sampled at 512 Hz. In this study, we divided the signals into five commonly investigated frequency bands: δ (0.4–4 Hz), θ (4–8 Hz), α (8–13 Hz), β (13–30 Hz), and γ (30–50 Hz). To evaluate the contribution of each frequency band to classification performance, the signals from 15 channels were replicated five times, resulting in multi-band datasets. These replicated data from each channel were subjected to bandpass filters with five different ranges: δ , θ , α , β , and γ . Notably, the δ band typically includes frequencies between 0 Hz and 4 Hz, but in our study, the filter range was adjusted to 0.4–4 Hz to reduce movement-induced noise. After filtering, linear-type detrending was applied, followed by outlier removal using the z-score method with a threshold of three

standard deviations. Cubic interpolation was used for interpolation. The signals were normalized to achieve a zero mean and a standard deviation of one to reduce inter-subject variability. Signal preprocessing was conducted using Python 3.7.12 with SciPy 1.7.3.

2.3. Deep learning

2.3.1 EEGNet

EEGNet is a compact and efficient CNN-based classifier designed for EEG signal analysis. It achieves superior performance compared to traditional methods while noticeably reducing the number of trainable parameters, making it ideal for analyzing EEG data effectively. EEGNet architecture has been extensively validated across various studies, demonstrating its efficacy in diverse scenarios owing to its lightweight design and ease of implementation [20,21].

In this study, the EEGNet classifier processed two-dimensional (2D) ECoG signals as inputs, comprising temporal (horizontal axis) and spatial (vertical axis) features, and classified the data into two states: pre-stimulation and post-stimulation. Each sample of data, six-second long, was segmented without overlap from a preprocessed 30-min long signal. Each sample included six-second long segments from multi-band datasets, which were composed of five frequency bands across 15 channels. We employed five-fold cross validation (CV) and divided the entire dataset into five folds. In each iteration, one fold was used as a test set, 10% of the remaining four folds were used for validation, and the other 90% were used for training. This process was repeated five times, with each fold being used exactly once as the test set. For model training, we used an Adam optimizer with a fixed learning rate of 0.001. A batch size of 16 was used. We trained for 100 epochs using training data. The model with the smallest validation loss was selected.

One of the best strategies to build a classifier is to gather a large number of subjects and train the classifier in a subject-independent manner. This approach allows the classifier to learn general features by using all available data. Unfortunately, it was challenging to increase the number of subjects in this study because of difficulties in modeling PD in rats and the high cost of electrodes. Consequently, we trained a classifier for each individual subject using a subject-dependent approach and analyzed whether each classifier showed consistent trends. The average accuracy of the 5-fold test for each of the four rats was over 0.99, indicating

exceptionally high performance.

The EEGNet architecture adopted in this study is depicted in Figure 1C. This model comprises three primary blocks. The initial layer of the first block is a 2D convolutional layer, which generates feature maps capturing characteristics from various frequency bands through convolution properties. Here, the model acquires knowledge of features across diverse frequency ranges, followed by batch normalization. In the subsequent depthwise convolution layer, spatial filters are learned for each feature map individually, enabling the model to learn frequency-specific spatial filters. This is succeeded by another batch normalization, an activation layer, average pooling layer, and dropout. The second block comprises a separable convolution layer, subsequently followed by batch normalization, activation, average pooling, and dropout. The separable convolution layer combines depthwise convolution and pointwise convolution, with the former summarizing the features for each feature map and the latter combining these summarized features. The final block, the classifier block, involves flattening the output from the second block and passing it through a dense network to classify the data [16].

2.3.2 Layer-wise Relevance Propagation

We used Layer-wise Relevance Propagation (LRP) [22] to determine which channel the model focuses on when classifying pre- and post-stimulation in Parkinsonian rats. LRP, a well-known framework in the field of XAI, decomposes the relevance score from the network's output backward through to the input layer. This process analyzes how each input feature contributes to the network's prediction. When redistributing the relevance score in LRP, the following rule is applied, known as the naive rule [23]. The relevance score R_i^l for neuron i in layer l is given by the following equation:

$$R_i^l = \sum_j \frac{z_{ij}}{\sum_{i'} z_{i'j}} R_j^{(l+1)} \quad \text{with} \quad z_{ij} = x_i^{(l)} w_{ij}^{(l,l+1)}$$

Here, l indexes the layer, i indexes the neurons in layer l , and j indexes the neurons in layer $l + 1$. The term R_i^l represents the relevance score of neuron i in layer l . The term z_{ij} is the product of the activation value $x_i^{(l)}$ of neuron i in layer l and the weight $w_{ij}^{(l,l+1)}$ from neuron i in layer l to neuron j in layer $l + 1$. This product z_{ij} indicates how much

neuron i contributes to the activation of neuron j in the next layer. The denominator $\sum_{i'} z_{i'j}$ represents the sum of contributions z from all neurons i' in layer l to neuron j in layer $l + 1$, serving as a normalization factor. This normalization ensures that the relevance score is distributed proportionally to the contribution of each neuron. When this redistribution algorithm is applied, it produces a relevance map (or heatmap) that satisfies the conservation property $\sum_p R_p^{(1)} = f(x)$, where $R_p^{(1)}$ denotes the relevance score for the p th input feature in the first layer, representing how much the p th input feature contributes to the overall output of the network. In other words, the total relevance score assigned to all input features is equal to the network's output value.

The ϵ -rule is a variant of the naive redistribution rule described above and is expressed as:

$$R_i^l = \sum_j \frac{z_{ij}}{\sum_{i'} z_{i'j} + \epsilon \text{sign}(\sum_{i'} z_{i'j})} R_j^{(l+1)}$$

Here, $\epsilon > 0$ is introduced to prevent the denominator from becoming zero, thus ensuring numerical stability. It also has the effect of reducing the values of neurons with very small contributions, thereby removing noise from the explanation. However, unlike the naive rule, the ϵ -rule does not satisfy the conservation property.

When analyzing the relevance map, positive values indicate features that increase the prediction probability for a given sample, while negative values indicate features that decrease the prediction probability. Using the absolute values of the relevance scores allows us to emphasize the magnitude of the feature's influence, regardless of whether it is positive or negative. Features with values close to zero have little impact on the model's decision, whereas features with larger absolute values have a higher impact on the model's decision. Therefore, the relevance map with absolute values can indicate how much the model relies on specific features. We divided each channel into five frequency bands through preprocessing and analyzed the importance by channel as well as band. For example, the XAI analysis block of Figure 1C depicts the heat map of input data and the relevance map obtained through LRP. We analyzed all relevance maps of true positive (TP) samples to determine the trend of feature importance across frequency bands and channel positions for distinguishing post-stimulation samples.

2.4. Statistical analysis

Statistical analysis was performed using SPSS 28.0 (IBM Corp., Armonk, NY, USA). Data were expressed as mean \pm standard error (SEM). The pre-stimulation and post-stimulation groups were compared using a one-tailed paired t-test. Comparisons involving three or more groups were analyzed using a one-way analysis of variance (ANOVA) with Bonferroni post hoc test. Statistical significance was defined as $p < 0.05$, with symbols denoting significance levels ($*p < 0.05$, $**p < 0.01$, $***p < 0.005$, $****p < 0.001$). Graphs were created using GraphPad® Prism 7 (GraphPad Software Inc., La Jolla, CA). Illustrations were produced using Illustrator CC 2021 (Adobe Inc., San Jose, CA) and Biorender.com. Power spectral density (PSD) estimation was conducted using Welch's method in Python 3.7.12 with SciPy 1.7.3. The band power ratio for each frequency band was calculated by summing the PSD values corresponding to each band and dividing by the total sum of the PSD values.

3. Results

Section 3.1 presents the experimental settings, including the classifiers and the input data format. Section 3.2 validates the reliability of the ECoG signals from Parkinsonian rats in response to electrical stimulation by analyzing their PSD using a conventional statistical method. In Section 3.3, we describe how XAI is used to investigate the changes in brain waves before and after the stimulation, considering channel location and frequency band. Finally, Section 3.4 examines how the XAI-based analysis results change with variations in the sample window size.

3.1 Experimental settings

To analyze the importance of each frequency band, the ECoG signals from the 15 original channels were each replicated five times, resulting in a total of 75 multi-band datasets. These expanded datasets were then subjected to the bandpass filters corresponding to the five main brainwave bands: δ , θ , α , β , and γ . The channels were grouped into four areas based on the motor cortex map: Area 1 (face), Area 2 (forelimb), Area 3 (trunk), and Area 4 (hindlimb), as described in the Methods section [26].

Each input sample was six-second long and segmented without overlap from the preprocessed signals. We employed EEGNet to analyze these input data [20,21]. The network structure followed the specifications presented in the original paper [16], and the kernel size for the temporal convolutional layer was set to (1×256) , which is half of the sampling rate. Four Parkinsonian rats were studied. Given the limited number of subjects, the classifiers were trained subject-dependently. To eliminate bias from dataset selection, a 5-fold CV was employed, training five classifiers for each rat.

3.2. Statistical analysis based on PSD

We conducted mean comparison analyses of PSD between pre-stimulation (pre-stim) and post-stimulation (post-stim) phases. Mean comparison analyses is a conventional statistical analysis that allows us to observe how brainwave activity in different frequency bands changes before and after stimulation in Parkinsonian rats. For Figures 2A and 2B, a one-sided paired t-test was performed on the PSD to compare pre- and post-stimulation. For Figure 2C, one-way ANOVA was used to compare the changes of PSD among the frequency bands. All PSD data are derived from preprocessed ECoG data using Fourier transform.

First, we compared the pre- and post-stimulation using the averages calculated across all electrode channels. Figure 2A shows the changes in the PSD between pre- and post-stimulation, which was evaluated from all 15 channels and four subjects. Statistically significant changes were observed in the δ , β , and γ bands, with an increase in the ratio of the δ band and a decrease in the ratio of the β and γ bands. These findings are consistent with previous studies that showed decreased neural activity in high frequency bands following electrical stimulation in Parkinsonian rats, further validating our results [9,11,12].

Then, a PSD comparison was performed considering the electrode positioning to identify which brain region exhibited the most significant changes between pre- and post-stimulation (Figure 2B). We compared the PSD for each area and frequency band before and after stimulation, which was evaluated from all four subjects (Figure 2B). The trend of PSD changes before and after stimulation was consistent with that shown in Figure 2A. After the stimulation, the mean PSD in the δ band increased across all areas compared to pre-stimulation, while those in the β and γ bands decreased across all areas. However, no statistically significant differences in PSD between pre- and post-stimulation were observed across all areas and

frequency bands.

Finally, for each area, we investigated whether the pre- and post-stimulation differences in PSD were affected by the frequency band (Figure 2C). The PSD values were log-transformed, and the differences between pre- and post-stimulation were calculated. These values were then used for one-way ANOVA. The δ band exhibited a positive value (increase) in Areas 3 and 4, while the β and γ bands showed a negative value (decrease) in all areas, similar to the results shown in Figure 2B. However, no statistically significant changes across the frequency bands were observed in any area.

In summary, after the stimulation, there was a tendency for decreased neural activity in high-frequency bands, β and γ , and increased activity in the δ band across all areas. However, statistically significant changes between pre- and post-stimulation were observed only when the mean PSD values were evaluated across all areas. When the analysis was conducted separately for each area to distinguish electrode positions, the differences between pre- and post-stimulation were not significant. Finally, the effect of frequency bands on PSD differences was not statistically significant.

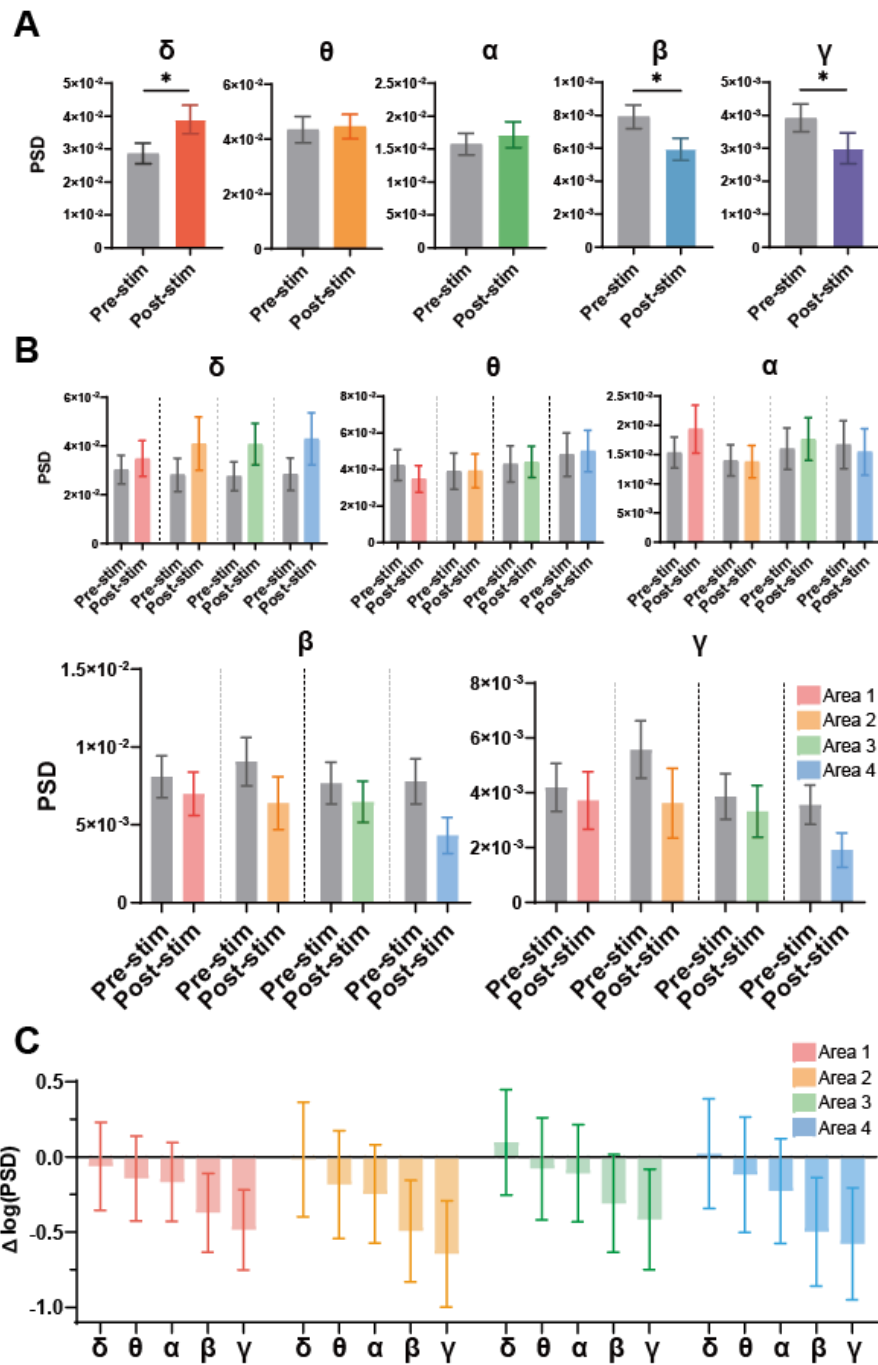


Figure 2. Effect of electrical stimulation on Parkinsonian rats was analyzed based on the ratio of each band power to the total power. (A) Average of normalized PSD for each frequency band evaluated from all four subjects and 15 channels (n = 60). (B) Average of normalized PSD for each area and frequency band evaluated from all four subjects. The sample sizes for Areas 1, 2, 3, and 4 are 20, 12, 16, and 12, respectively. (C) Changes in PSD between pre- and post-stimulation for each area. Statistical significance is indicated by $*p < 0.05$. All data are presented as the mean \pm SEM.

3.3. XAI-based analysis

Figure 3 presents an example comparing between preprocessed ECoG signals and relevance maps derived from them. The relevance map visualizes the importance of each ECoG signal sample during classification by the trained model, presented in the form of a heatmap. The left heatmap displays a one-second segment of absolute preprocessed ECoG signals, while the right heatmap shows the corresponding relevance map. The vertical axis represents the frequency bands, δ , θ , α , β , and γ , each subdivided into 15 channels, and the horizontal axis represents time in seconds. All data were extracted from PD2. Additional examples from other subjects are included in Supplementary Figure S1.

Figure 3 highlights the model's tendency to assign higher importance to features in the β and γ bands, a trend consistently observed across samples in the same subject and across all subjects. While one might expect that regions with the largest signal changes would have the highest relevance for the model's classification of pre- and post-stimulation phases, the relevance scores reveal a different pattern. More specifically, the heatmap trends of signal changes do not align with those of relevance scores, which only emphasize β and γ bands while showing little attention to other bands, highlighting high-frequency components. For example, in Figure 3, substantial changes in ECoG signals were observed in the α band, but it received relatively less attention in the relevance map. The γ band had relevance scores 3.01 times higher than the α band during the pre-stimulation and 4.99 times higher during the post-stimulation. The β band also showed scores 2.5 times higher than the α band before stimulation and 4.04 times higher afterward.

These results demonstrate XAI's ability to identify key frequency bands for distinguishing between pre- and post-stimulation without relying on traditional feature extraction methods such as Fourier transform. Interestingly, the frequency bands identified as most relevant by the XAI method align with the results obtained through statistical comparisons based on Fourier transform (Figure 2A).

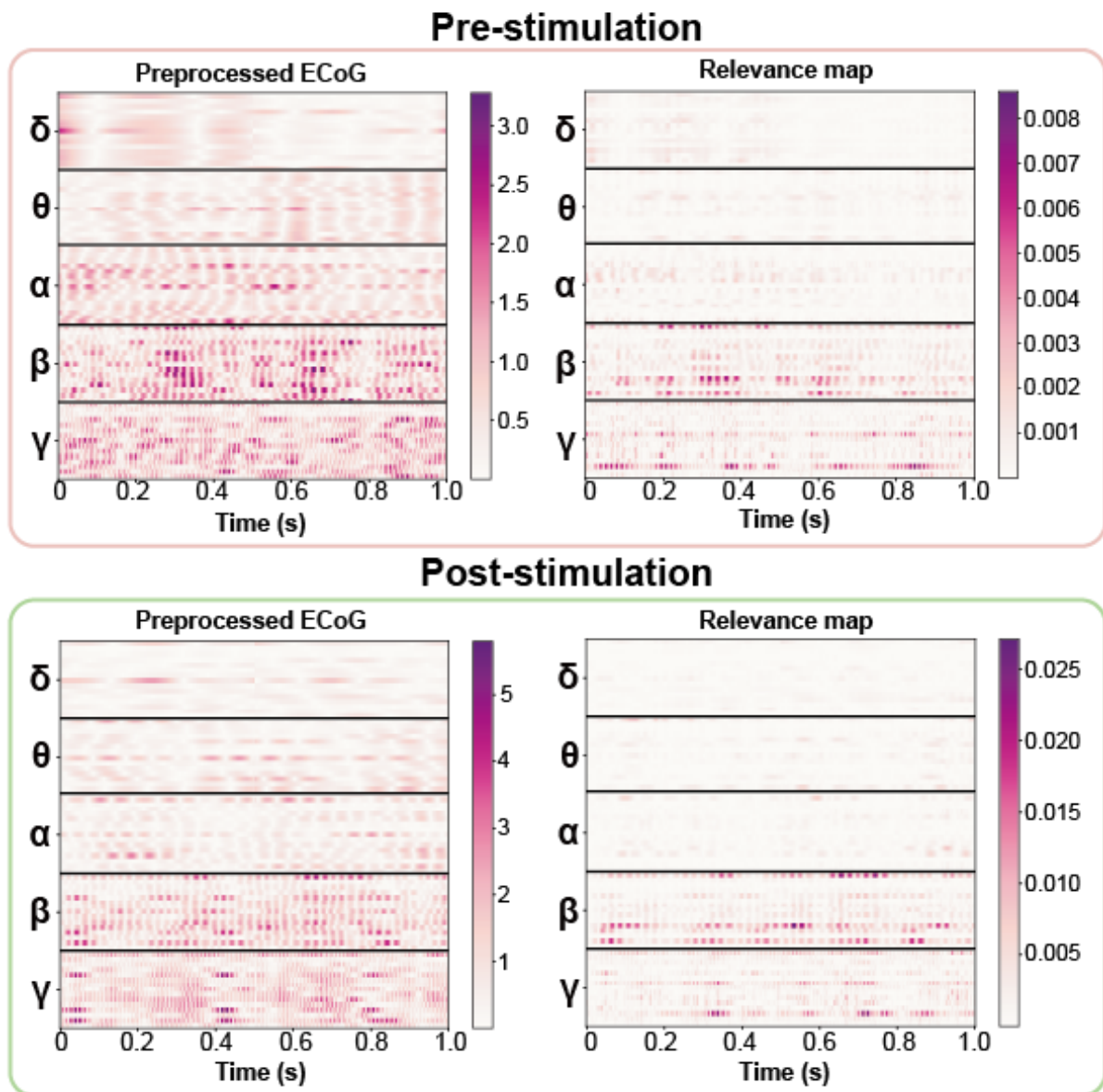


Figure 3. Comparison of ECoG signal and XAI relevance map. The left heatmap shows the normalized absolute values of the preprocessed ECoG signal. The right heatmap displays the XAI-based relevance map, highlighting the absolute relevance values of features used for classification. Both heatmaps correspond to the same sample.

In Figure 4, we investigate the significance of channel location and frequency band in differentiating between pre- and post-stimulation by calculating the absolute sum of relevance scores for TPs. TPs refer to the samples from the post-stimulation condition that were accurately classified by a classifier trained with each individual rat's data explicitly. For instance, the first plot in Figure 4A displays the LRP results for the samples correctly classified

as post-stimulation using a classifier trained specifically on the PD1 rat's data. Focusing only on the TPs, this analysis helps identify which features played a key role in the classifier's decision to label a particular sample as post-stimulation.

Figure 4A shows the normalized relevance score for each channel, which was evaluated by summing up all samples for each channel, then normalizing the data by dividing each sum by the maximum sum across all channels. The heatmap is designed to reflect the actual electrode positions, allowing us to identify which positions have the most significant impact on the model's classification results. Our analysis reveals that numerous channels exhibit higher values in the γ band compared to other bands.

Figure 4B depicts the sum of absolute relevance scores obtained from all channels, evaluated for each frequency band. It shows that the values in the β and γ bands are consistently higher for all subjects. However, in the PD3 rat, the values in the β band seem relatively less prominent because of the more pronounced changes in the δ band. The increased values in the δ band cause the values in the β band to appear relatively lower. Furthermore, the values in the θ and α bands are substantially lower compared to other subjects. Note that the prominence of the δ band in the PD3 rat reflects the unique characteristics of the subject, demonstrating that the analysis using XAI models can also capture low-frequency features effectively.

Figure 4C presents the mean and SEM of the sum of absolute relevance scores obtained from all channels, evaluated for each area and frequency band from all subjects. We used one-way ANOVA followed by Bonferroni post-hoc tests to compare the mean values among the frequency bands within each area group. We found that frequency bands significantly influenced the absolute relevance scores. In particular, the γ band shows significantly higher values compared to other frequency bands in Areas 1, 3, and 4. This finding contrasts with Figure 2C, where frequency bands had no significant effect on PSD changes. This highlights the XAI model's ability to identify biomarkers more effectively than traditional analysis.

In summary, the results based on LRP indicate that the β and γ bands play an important role in the model's classification. This aligns with existing studies demonstrating that the changes in high-frequency bands are pronounced following electrical stimulation in Parkinsonian rats [4,24,25]. Furthermore, the XAI-based analysis identified significant differences in importance between frequency bands while incorporating spatial information, which were not detected in the PSD-based statistical test.

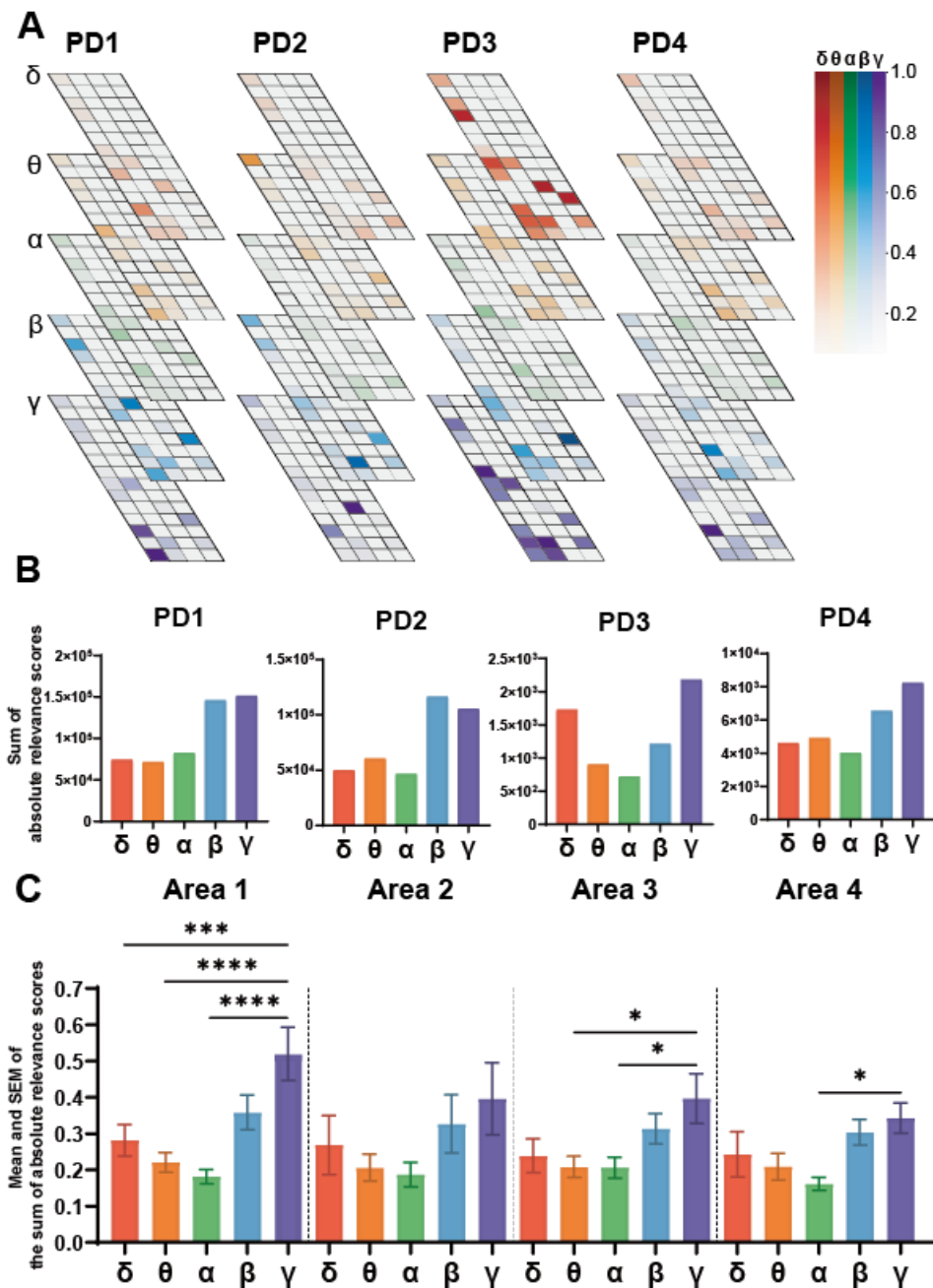


Figure 4. Analysis of importance based on relevance scores obtained using LRP from each individual rat. (A) Heatmap representation of normalized relevance scores evaluated separately by channel locations and frequency bands. Each cell in the matrix represents the absolute sum of relevance scores for a specific electrode channel at a particular frequency band, normalized by the maximum value observed across all channels. (B) Sum of absolute relevance scores obtained from all channels, evaluated for each frequency band. (C) Mean and SEM of the sum of absolute relevance scores obtained from all channels, evaluated for each area and frequency band from all subjects. * $p < 0.05$, *** $p < 0.005$, **** $p < 0.001$.

3.4. Effect of window size on the relevance scores

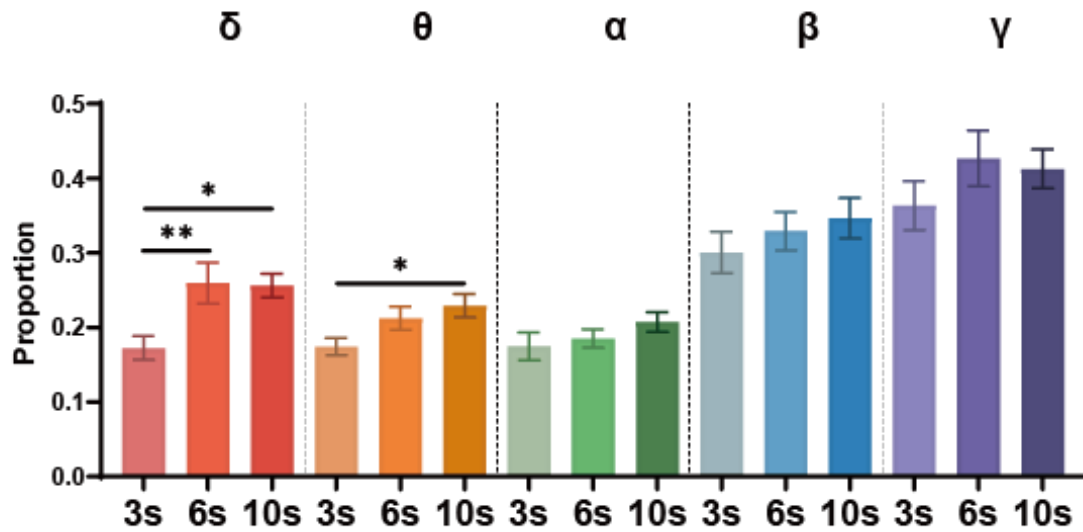


Figure 5. Proportion of each frequency band in the total sum of the absolute relevance scores, which was evaluated for each window size. Each bar represents the mean and SEM across all 15 channels and four subjects (n = 60).

In determining the window size for data samples, several factors must be accounted for. A smaller window size increases the number of data samples, which can help the model learn effectively with limited data. However, the shorter sample length may not be adequate for capturing the characteristics of low-frequency bands. Conversely, a larger window size allows the model to effectively learn the features of low-frequency bands, but it reduces the number of data samples, potentially resulting in various side effects during model training. Therefore, it is essential to establish a window size that enables the model to effectively capture the characteristics of low-frequency bands while maximizing the number of data samples.

In this study, the lowest frequency considered is 0.4 Hz, which requires a minimum data length of 2.5 seconds to ensure adequate frequency resolution. With a total data length of 30 minutes, a window size of 3 seconds would yield 600 samples, but was considered too short. A window size of 10 seconds would provide sufficient data length, but only 180 samples could be obtained. Therefore, we opted for a compromise and set the window size to 6 seconds for our experiments.

In order to examine the influence of window size on the outcomes, we conducted a comparative analysis using window sizes of 3, 6, and 10 seconds. Figure 5 depicts the proportion of each frequency band in the total sum of the absolute relevance scores, which was

evaluated for each window size using LRP. This allows us to identify changes in each frequency band depending on the window size. A one-way ANOVA followed by Bonferroni post hoc test was performed for each frequency band to test the effect of the various window sizes.

Analysis results indicated that the lowest frequency band, the δ band, exhibited significant changes when the window size was adjusted from 3 seconds to 6 seconds. However, no significant differences were observed when increasing the window size from 6 seconds to 10 seconds. Based on this, a 6-second window size was chosen for our research, as it allows for a sufficient number of samples and effectively captures the characteristics of the low-frequency band.

4. Limitations

A major limitation of this study is the small number of subjects. The invasiveness and complexity of surgical procedure and ECoG acquisition, high costs, and ethical concerns posed challenges in data collection from a large number of subjects. Consequently, we had to conduct our study using a subject-dependent approach, which is a key reason why our findings may not be generalizable to other subjects. Furthermore, assessing the importance of specific brain regions based on channel locations involves various factors, such as inter-subject difference (e.g., brain size) and subtle inconsistency during electrode placement. The limited number of subjects makes it difficult to ignore these variables, which may introduce bias into the analysis results.

Another limitation of our study is that we only utilized a single XAI algorithm. Using just one XAI algorithm poses the risk of generating results that are biased by the unique characteristics of that algorithm. Different XAI algorithms can offer different explanations for the same model. Therefore, it is essential to try multiple algorithms to obtain results from various perspectives and ensure the reliability of the findings. Our future research will address these issues to improve the reliability and generalizability of XAI-based brain wave analysis frameworks.

5. Conclusion

We demonstrated that XAI-based analytical methods can provide reliable analysis

results without the need for handcrafted features. To validate the effectiveness of XAI analysis on biological data, we conducted a study based on the existing knowledge that high-frequency bands show substantial differences before and after electrical stimulation in the Parkinsonian rat model [4,24,25]. Our study demonstrated significant differences in the high-frequency bands between pre- and post-stimulation using conventional PSD-based statistical comparisons, which aligns with previous literature. Similarly, the XAI-based analysis focused on changes in high-frequency bands. In addition, XAI was able to learn the changes in the signals that handcrafted features like PSD could not capture. It revealed significant differences in the importance between frequency bands while considering spatial information, which was not detected through the PSD-based statistics alone. Furthermore, we observed the changes in analysis results based on the window size, the most critical hyperparameter in XAI-based analysis, and selected an optimal window size that efficiently captures the characteristics of low-frequency bands while also ensuring a sufficient number of samples. The proposed XAI-based classification framework for PD is expected to enable real-time use of relevance scores to distinguish pre- and post-stimulation states. This capability could support the autonomous determination of optimal stimulation timing, potentially eliminating the need for manual intervention and improving the efficiency of therapy.

CRedit authorship contribution statement

Jibum Kim: Conceptualization, Writing – Review & Editing, Supervision, Project administration, Funding acquisition. **Hanseul Choi:** Methodology, Software, Investigation, Writing - Original Draft. **Gaeun Kim:** Methodology, Formal analysis, Visualization, Writing - Original Draft. **Sunggu Yang:** Resources, Data Curation, Funding acquisition. **Eunha Baeg:** Data Curation, Writing - Review & Editing. **Donggue Kim:** Formal analysis, Visualization, Writing - Review & Editing. **Seongwon Jin:** Investigation. **Sangwon Byun:** Methodology, Validation, Writing - Review & Editing, .

Data Availability

The data that support the findings of this study are partially available from the corresponding author upon reasonable request

Acknowledgments

This work was supported in part by the MSIT (Ministry of Science and ICT), Korea, under the ICAN (ICT Challenge and Advanced Network of HRD) support program (IITP-2024-RS-2023-00260175, 50%) supervised by the IITP (Institute for Information & Communications Technology Planning & Evaluation). This work was also supported by Incheon National University Research Grant in 2024.

References

- [1] L.M.L. de Lau, and M.M.B. Breteler, Epidemiology of Parkinson's disease, *Lancet Neurol.* 5 (6) (2006) 525-535. [https://doi.org/10.1016/S1474-4422\(06\)70471-9](https://doi.org/10.1016/S1474-4422(06)70471-9).
- [2] S. Sveinbjornsdottir, The clinical symptoms of Parkinson's disease, *J. Neurochem.* 139 (2016) 318-324. <https://doi.org/10.1111/jnc.13691>.
- [3] B.R. Bloem, M.S. Okun, C. Klein, Parkinson's disease, *Lancet* 397 (10291) (2021) 2284-2303. [https://doi.org/10.1016/S0140-6736\(21\)00218-X](https://doi.org/10.1016/S0140-6736(21)00218-X).
- [4] C. de Hemptinne, N.C. Swann, J.L. Ostrem, et al., Therapeutic deep brain stimulation reduces cortical phase-amplitude coupling in Parkinson's disease, *Nat. Neurosci.* 18 (5) (2015) 779–786. <https://doi.org/10.1038/nn.3997>
- [5] J. Lim, S. Lee, J. Hong, et al., 2023, Hybrid graphene electrode for the diagnosis and treatment of epilepsy in free-moving animal models. *NPG Asia Mater.* 15 (1), 7. <https://doi.org/10.1038/s41427-023-00464-1>.
- [6] M. Lee, S. Lee, J. Kim, et al., 2021, Graphene-electrode array for brain map remodeling of the cortical surface. *NPG Asia Mater.* 13 (1), 65. <https://doi.org/10.1038/s41427-021-00334-8>.
- [7] S.W. Park, J. Kim, M. Kang, et al., 2018. Epidural electrotherapy for epilepsy. *Small.* 14 (30), 1801732. <https://doi.org/10.1002/sml.201801732>.
- [8] D. Kim, M. Jeong, E. Kim, et al., 2023. Brain mapping using a graphene electrode array. *J. Vis. Exp.* 200, e64910. <https://dx.doi.org/10.3791/64910>.
- [9] X. Jiang, J. Yang, Z. Wang, et al., 2024. Functional interaction of abnormal beta and gamma oscillations on bradykinesia in Parkinsonian rats. *Brain Res. Bull.* 209, 110911. <https://doi.org/10.1016/j.brainresbull.2024.110911>.
- [10] E.J. Müller, P.A. Robinson, 2018. Suppression of Parkinsonian beta oscillations by deep brain stimulation: determination of effective protocols. *Front. Comput. Neurosci.* 12, 98. <https://doi.org/10.3389/fncom.2018.00098>.
- [11] M. Beudel, S. Little, A. Pogosyan, et al., Tremor reduction by deep brain stimulation is associated with gamma power suppression in Parkinson's disease, *Neuromodulation* 18 (5) (2015) 349-354. <https://doi.org/10.1111/ner.12297>.

- [12] S. Sylvester, et al., SHAP value-based ERP analysis (SHERPA): Increasing the sensitivity of EEG signals with explainable AI methods, *Behav. Res. Methods* (2024) 1-15. <https://doi.org/10.3758/s13428-023-02335-7>.
- [13] I. Sturm, S. Lapuschkin, W. Samek, et al., Interpretable deep neural networks for single-trial EEG classification, *J. Neurosci. Methods* 274 (2016) 141–145. <https://doi.org/10.1016/j.jneumeth.2016.10.008>.
- [14] J.S. Bang, M.H. Lee, S. Fazli, et al., Spatio-spectral feature representation for motor imagery classification using convolutional neural networks, *IEEE Trans. Neural Netw. Learn. Syst.* 33 (7) (2021) 3038–3049. <https://doi.org/10.1109/TNNLS.2020.3048385>.
- [15] D. Wang, N. Honnorat, P.T. Fox, et al., 2023. Deep neural network heatmaps capture Alzheimer’s disease patterns reported in a large meta-analysis of neuroimaging studies. *Neuroimage*. 269, 119929. <https://doi.org/10.1016/j.neuroimage.2023.119929>.
- [16] V.J. Lawhern, A.J. Solon, N.R. Waytowich, et al., 2018. EEGNet: A Compact Convolutional Neural Network for EEG-based Brain-Computer Interfaces. *J. Neural Eng.* 15 (5), 056013. <https://doi.org/10.1088/1741-2552/ace8c>.
- [17] Y. R. Tabar, and U. Halici, 2016, A novel deep learning approach for classification of EEG motor imagery signals. *J. Neural Eng.* 14 (1), 016003. <https://doi.org/10.1088/1741-2560/14/1/016003>.
- [18] M. Böhle, F. Eitel, M. Weygandt, & K. Ritter, 2019. Layer-wise relevance propagation for explaining deep neural network decisions in MRI-based Alzheimer’s disease classification. *Front. Aging Neurosci.* 11, 456892. <https://doi.org/10.3389/fnagi.2019.00194>.
- [19] A. de Cheveigne, D. Arzounian, Robust detrending, rereferencing, outlier detection, and inpainting for multichannel data, *Neuroimage* 172 (2018) 903-912. <https://doi.org/10.1016/j.neuroimage.2018.01.035>.
- [20] Z. Lv, X. Liu, M. Dai, et al., 2024. Investigating critical brain area for EEG-based binocular color fusion and rivalry with EEGNet. *Front. Neurosci.* 18, 1361486. <https://doi.org/10.3389/fnins.2024.1361486>.
- [21] L. Feng, L. Yang, S. Liu, et al., 2022. An efficient EEGNet processor design for portable EEG-based BCIs. *Microelectron. J.* 120, 105356. <https://doi.org/10.1016/j.mejo.2021.105356>.
- [22] S. Bach, A. Binder, G. Montavon, et al., 2015. On pixel-wise explanations for non-linear classifier decisions by layer-wise relevance propagation. *PLoS One.* 10 (7), e0130140. <https://doi.org/10.1371/journal.pone.0130140>.
- [23] A. Binder, S. Bach, G. Montavon, et al., Layer-wise relevance propagation for deep neural network architectures, in: *Information science and applications (ICISA)*, Springer, 2016. pp. 913-922, https://doi.org/10.1007/978-981-10-0557-2_87.
- [24] J.L. Ulloa, 2022. The control of movements via motor gamma oscillations. *Front. Aging Neurosci.* 15, 787157. <https://doi.org/10.3389/fnhum.2021.787157>.
- [25] J. Barone, & H.E. Rossiter, 2021. Understanding the role of sensorimotor beta oscillations. *Front. Syst. Neurosci.* 15, 655886. <https://doi.org/10.3389/fnsys.2021.655886>.
- [26] Ebbesen, C. L., Insanally, M. N., Kopec, C. D., et al., 2018. More than just a “motor”: recent surprises from the frontal cortex. *J. Neurosci.* 38 (44), 9402-9413.

<https://doi.org/10.1523/JNEUROSCI.1671-18.2018>.